

Nanosecond Time-Dependent Stokes Shift at the Tunnel Mouth of Haloalkane Dehalogenases

Andrea Jesenská,[†] Jan Sýkora,[‡] Agnieszka Olżyńska,[‡] Jan Brezovský,[†]
Zbyněk Zdráhal,[§] Jiří Damborský,^{*,†} and Martin Hof^{*,‡}

Loschmidt Laboratories, Institute of Experimental Biology and National Centre for Biomolecular Research, Faculty of Science, Masaryk University, Kamenice 5/A4, 625 00 Brno, Czech Republic, J. Heyrovský Institute of Physical Chemistry of the ASCR, v. v. i., Dolejškova 3, 182 23 Prague 8, Czech Republic, and Department of Functional Genomics and Proteomics, Institute of Experimental Biology, Faculty of Science, Masaryk University, Kamenice 5/A2, 625 00 Brno, Czech Republic

Received May 29, 2008; E-mail: martin.hof@jh-inst.cas.cz; jiri@chemi.muni.cz

Abstract: The tunnel mouths are evolutionally the most variable regions in the structures of haloalkane dehalogenases originating from different bacterial species, suggesting their importance for adaptation of enzymes to various substrates. We decided to monitor the dynamics of this particular region by means of time-resolved fluorescence spectroscopy and molecular dynamic simulations. To label the enzyme specifically, we adapted a novel procedure that utilizes a coumarin dye containing a halide–hydrocarbon linker, which serves as a substrate for enzymatic reaction. The procedure leads to a coumarin dye covalently attached and specifically located in the tunnel mouth of the enzyme. In this manner, we stained two haloalkane dehalogenase mutants, DbjA-H280F and DhaA-H272F. The measurements of time-resolved fluorescence anisotropy, acrylamide quenching, and time-resolved emission spectra reveal differences in the polarity, accessibility and mobility of the dye and its microenvironment for both of the mutants. The obtained experimental data are consistent with the results obtained by molecular dynamics calculations and correlate with the anatomy of the tunnel mouths, which were proposed to have a strong impact on the catalytic activity and specificity of the examined mutants. Interestingly, the kinetics of the recorded time-dependent Stokes shift is unusual slow; it occurs on the nanosecond time-scale, suggesting that the protein dynamics is extremely slowed down at the region involved in the exchange of ligands between the active-site cavity and bulk solvent.

Introduction

The study of the solvation dynamics¹ at the protein surface as well as in the protein interior is of large scientific interest,^{2–4} and has been studied by means of NMR,⁵ neutron scattering,⁶ and computer simulations.⁷ For example, Halle and co-workers^{5,7} showed that water molecules in the hydration layer of the protein surface were only slightly perturbed and more than 95% of them were not more than 2-fold motionally retarded in comparison to bulk water. In addition, in a series of time-resolved

fluorescence experiments^{8–12} the probe was attached to the protein surface and the time-dependent Stokes shift (TDSS) was recorded. TDSS characterizes the overall red-shift of the time-resolved fluorescence spectra caused by the reorientation motions of the solvent dipoles provoked by a sudden change in the charge distribution of the excited solute molecule. Explicitly, it follows the evolution of the time-resolved spectra starting from the spectrum recorded for the initial Franck–Condon state up to the spectrum corresponding to the final completely relaxed state. Specifically, the time scale of the probed dynamics in this region was found to be in the range of picoseconds.^{8–14} However, those studies investigating the dynamics close to the

[†] Loschmidt Laboratories, Institute of Experimental Biology and National Centre for Biomolecular Research, Faculty of Science, Masaryk University.

[‡] J. Heyrovský Institute of Physical Chemistry of the ASCR.

[§] Department of Functional Genomics and Proteomics, Institute of Experimental Biology, Faculty of Science, Masaryk University.

- (1) Jimenez, R.; Fleming, G. R.; Kumar, P. V.; Maroncelli, M. *Nature* **1994**, *369*, 471–473.
- (2) Bhattacharyya, K. *Acc. Chem. Res.* **2003**, *36*, 95–101.
- (3) Pal, S. K.; Zewail, A. H. *Chem. Rev.* **2004**, *104*, 2099–2123.
- (4) Nandi, N.; Bhattacharyya, K.; Bagchi, B. *Chem. Rev.* **2000**, *100*, 2013–2045.
- (5) Modig, K.; Liepinsh, E.; Otting, G.; Halle, B. *J. Am. Chem. Soc.* **2004**, *126*, 102–114.
- (6) Dellerue, S.; Bellissent-Funel, M. C. *Chem. Phys.* **2000**, *258*, 315–325.
- (7) Nilsson, L.; Halle, B. *Proc. Natl. Acad. Sci. U.S.A.* **2005**, *102*, 13867–13872.

- (8) Abbyad, P.; Shi, X. H.; Childs, W.; McAnaney, T. B.; Cohen, B. E.; Boxer, S. G. *J. Phys. Chem. B* **2007**, *111*, 8269–8276.
- (9) Chagnenet-Barret, P.; Choma, C. T.; Gooding, E. F.; DeGrado, W. F.; Hochstrasser, R. M. *J. Phys. Chem. B* **2000**, *104*, 9322–9329.
- (10) Sen, P.; Mukherjee, S.; Dutta, P.; Halder, A.; Mandal, D.; Banerjee, R.; Roy, S.; Bhattacharyya, K. *J. Phys. Chem. B* **2003**, *107*, 14563–14568.
- (11) Lundgren, J. S.; Heitz, M. P.; Bright, F. V. *Anal. Chem.* **1995**, *67*, 3775–3781.
- (12) Sahu, K.; Mondal, S. K.; Ghosh, S.; Roy, D.; Sen, P.; Bhattacharyya, K. *J. Phys. Chem. B* **2006**, *110*, 1056–1062.
- (13) Dutta, P.; Sen, P.; Haider, A.; Mukherjee, S.; Sen, S.; Bhattacharyya, K. *Chem. Phys. Lett.* **2003**, *377*, 229–235.
- (14) Mondal, S. K.; Roy, D.; Sahu, K.; Mukherjee, S.; Halder, A.; Bhattacharyya, K. *J. Mol. Liq.* **2006**, *124*, 128–135.

protein surface do have, in fact, very little implication for the function of the investigated proteins, and only few papers can be found performing time-dependent fluorescence studies on the water dynamics at deeper buried sites with a relevancy for the biological activity of the protein.^{10,15–18} For instance, Petrich et al. investigated the transient Stokes shift in the pocket of the heme-containing protein and did report subpicosecond relaxation processes for the probed interior of the protein.¹⁶ In contrast, significantly slower solvation response processes on the nanosecond time scale were found by Bhattacharyya and co-workers¹⁵ who studied solvation dynamics with the fluorescent dye most probably covalently attached in the vicinity of the enzyme active site. They reported the existence of two relaxing components on the order of hundreds of picoseconds and units of nanoseconds, whereas less than 40% of the TDSS response was happening on the shorter time scales. The cause for such disparate results may originate from the fact that some fraction of the dye molecules was nonspecifically bound to the investigated protein. As the recorded TDSS is highly dependent on the distribution of the probe locations, the labeling procedure used shall guarantee a single location of the dye contributing to the detected TDSS.

Therefore, in this contribution we adapt a novel approach for labeling enzymes site-specifically at the entry to the active site, thus, being able to get defined information on the protein dynamics at that site. Specifically, we are monitoring the TDSS of a coumarin dye located at the tunnel mouth toward the active site of two different haloalkane dehalogenases, DbjA from *Bradyrhizobium japonicum* USDA110¹⁹ and DhaA from *Rhodococcus rhodochrous* NCIMB13064.²⁰ DbjA and DhaA enzymes possess different substrate specificities, which are due to the differences in the active sites as well as access tunnels connecting the active-site cavities with the protein surface.^{21,22}

Haloalkane dehalogenases (EC 3.8.1.5) catalyze hydrolytic cleavage of carbon–halogen bonds in halogenated aliphatic compounds, producing a corresponding alcohol, a halide ion, and a proton.²³ The structures of these enzymes consist of an α/β -hydrolase fold domain and a helical cap domain.^{24,25} The active site is deeply buried in a protein core and contains a catalytic triad consisting of a nucleophilic aspartate, an adjacent histidine that acts as the catalytic base, and a glutamate residue that serves as the catalytic acid. A reaction mechanism of dehalogenation involves a nucleophilic attack of the carboxylate

oxygen of an aspartate group on the carbon atom of the substrate, yielding displacement of the halogen as the halide and formation of a covalent alkyl-enzyme intermediate.²⁶ The alkyl-enzyme intermediate is subsequently hydrolyzed by a water molecule which is activated by the catalytic histidine. A catalytic acid stabilizes the charge developed on the imidazole during the hydrolysis. The haloalkane dehalogenase carrying the mutation in the catalytic histidine forms the ester bond between the nucleophile and the substrate, which cannot be further hydrolyzed, providing the covalent alkyl-enzyme intermediate (Figure 1). Here, we took advantage of the covalent labeling of haloalkane dehalogenase enzymes with the fluorescent coumarin dye²⁷ and developed a protocol that specifically labels the tunnel mouth toward the active sites with simultaneous elimination of all the unbound and nonspecifically bound dye molecules. The results gained by means of a solvent relaxation technique applied to such a system provide quantitative information on the hydration and mobility of the protein and monitor differences in probe microenvironments. Molecular dynamic simulations with the protein–probe complexes provide additional information for interpretation of fluorescence data and establish structure–function relationships.

Experimental Section

Construction of DhaA and DbjA Variants Carrying Mutation in the Catalytic Histidine. Mutant recombinant genes were obtained using a QuikChange Site-Directed Mutagenesis Kit (Stratagene, La Jolla, U.S.A.) according to manufacturer's instructions. Specific complementary primers (5'-CATCGGCCCGGGAT-TGTTCTACCTCCAGGAAG-3' and 5'-CTCGGCGCGGGAT-TGTTCTATCTGCAGGAGG-3') carrying substitution (in bold) were designed for mutagenesis of *dhaA* and *dbjA* recombinant genes, respectively. Plasmids pUC18-*dhaA* and pUC18-*dbjA* containing the sequence encoding for the histidine tail on the C-terminus of the resulting protein were used as the templates. Mutant recombinant genes *dhaA* and *dbjA* were subcloned into an expression vector pAQN²⁸ using *Bam*HI and *Hind*III restriction sites.

Expression of DbjA-H280F and DhaA-H272F in *Escherichia coli* and Purification. After verification of the sequence by DNA-sequencing, the plasmid was transformed into *E. coli* BL21 for protein expression. For overexpression, cells were grown at 37 °C to an optical density at 600 nm about 0.6 in Luria–Bertani (LB) medium (Sigma-Aldrich, St. Louis, U.S.A.) with ampicillin (100 μ g/mL). Protein expression was induced by adding IPTG to a final concentration 0.5 mM in LB medium. The temperature was decreased to 30 °C. Cells were harvested by 12 min centrifugation at 3700g after 4 h of cultivation and washed once with glycine buffer (0.1 M, pH 8.5) and then resuspended in the glycine buffer. Harvested cells were stored at –65 °C overnight. The defrosted culture was disrupted by sonication with Soniprep 150 (Sanyo Gallenkamp, Loughborough, U.K.), and the lysate was centrifuged at 21000g for one hour. The crude extract was applied on a nickel-nitrilotriacetic acid (Ni-NTA) Superflow column (QIAGEN, Hilden, Germany) equilibrated with purification buffer of pH 7.5 composed of 16.4 mM K₂HPO₄, 3.6 mM KH₂PO₄, and 0.5 M NaCl containing 10 mM imidazole. Unbound and weakly bound fractions were eluted with purification buffer with 50 mM imidazole. Histidine-tagged protein was eluted with purification buffer with 300 mM imidazole. The eluted protein was dialyzed against 50 mM phosphate buffer composed of 41 mM K₂HPO₄ and 9 mM KH₂PO₄ (pH 7.5). Protein concentration was determined by the method of Bradford (Sigma-

- (15) Guha, S.; Sahu, K.; Roy, D.; Mondal, S. K.; Roy, S.; Bhattacharyya, K. *Biochemistry* **2005**, *44*, 8940–8947.
- (16) Halder, M.; Mukherjee, P.; Bose, S.; Hargrove, M. S.; Song, X. Y.; Petrich, J. W. *J. Chem. Phys.* **2007**, *127*, 0551011–6.
- (17) Toptygin, D.; Savtchenko, R. S.; Meadow, N. D.; Brand, L. *Biophys. J.* **2001**, *80*, 361A–361A.
- (18) Riter, R. R.; Edington, M. D.; Reck, W. F. *J. Phys. Chem.* **1996**, *100*, 14198–14205.
- (19) Sato, Y.; Monincova, M.; Chaloupkova, R.; Prokop, Z.; Ohtsubo, Y.; Minamisawa, K.; Tsuda, M.; Damborsky, J.; Nagata, Y. *Appl. Environ. Microbiol.* **2005**, *71*, 4372–4379.
- (20) Kulakova, A. N.; Larkin, M. J.; Kulakov, L. A. *Microbiology* **1997**, *143*, 109–115.
- (21) Marek, J.; Vevodova, J.; Kuta-Smatanova, I.; Nagata, Y.; Svensson, L. A.; Newman, J.; Takagi, M.; Damborsky, J. *Biochemistry* **2000**, *39*, 14082–14086.
- (22) Petrek, M.; Otyepka, M.; Banas, P.; Kosinova, P.; Koca, J.; Damborsky, J. *BMC Bioinformatics* **2006**, *7*, 316.
- (23) Janssen, D. B. *Curr. Opin. Chem. Biol.* **2004**, *8*, 150–159.
- (24) Nardini, M.; Dijkstra, B. W. *Curr. Opin. Struct. Biol.* **1999**, *9*, 732–737.
- (25) Ollis, D. L.; Cheah, E.; Cygler, M.; Dijkstra, B.; Frolow, F.; Franken, S. M.; Harel, M.; Remington, S. J.; Silman, I.; Schrag, J.; Sussman, J. L.; Verschuere, K. H. G.; Goldman, A. *Protein Eng.* **1992**, *5*, 197–211.

- (26) Verschuere, K. H. G.; Seljee, F.; Rozeboom, H. J.; Kalk, K. H.; Dijkstra, B. W. *Nature* **1993**, *363*, 693–698.

- (27) Los, G. V.; Wood, K. *Methods Mol. Biol.* **2007**, *356*, 195–208.

- (28) Nagata, Y.; Hynkova, K.; Damborsky, J.; Takagi, M. *Protein Expr. Purif.* **1999**, *17*, 299–304.

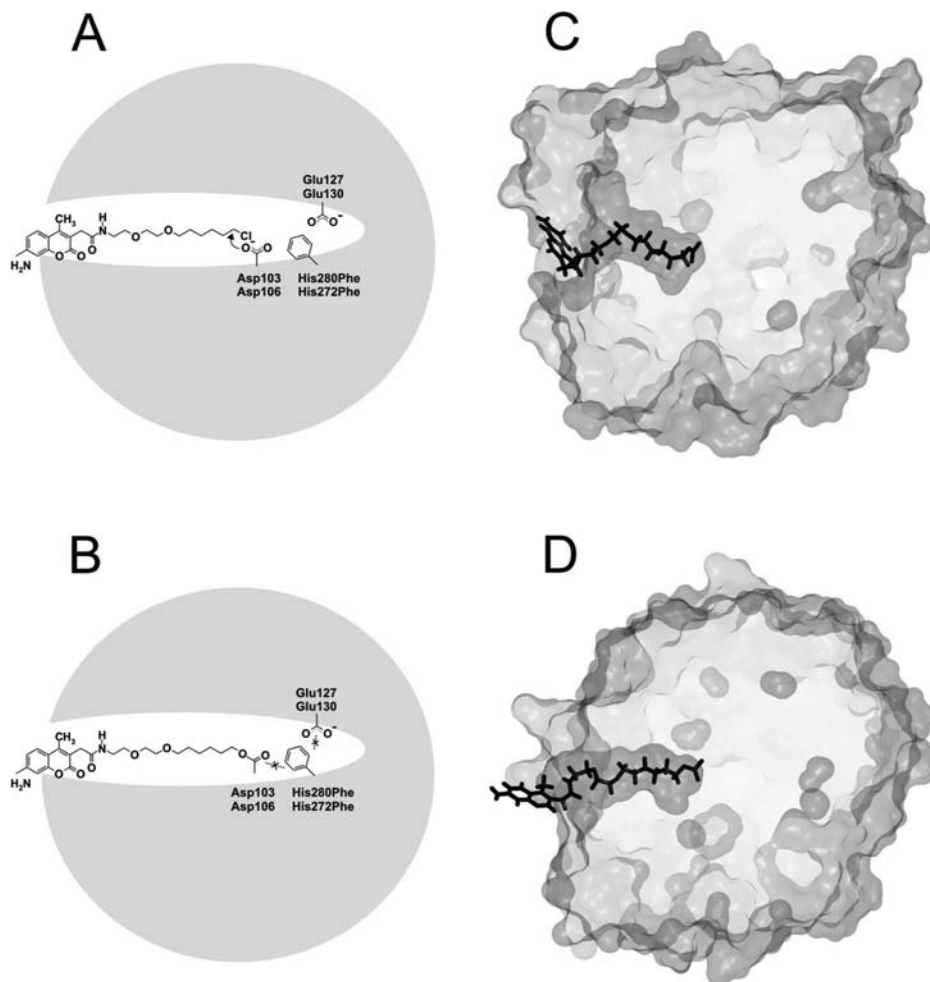


Figure 1. Molecular system of the haloalkane dehalogenase covalently linked to the fluorescent probe. Schematic representation of the formation of the covalent ligand–protein complex between the mutant haloalkane dehalogenase and the coumarin dye (A and B). Structural representation of the haloalkane dehalogenases DbjA (C) and DhaA (D) covalently linked to the coumarin dye. Complexes were prepared by the molecular docking of the coumarin probe to the respective crystal structures. Proteins are represented by a transparent molecular surface and coumarin dye by a black stick.

Aldrich, St. Louis, U.S.A.). Protein purity and size were verified by sodium dodecyl sulfate–polyacrylamide gel electrophoresis (SDS–PAGE).

Labeling of DbjA-H280F and DhaA-H272F by a Coumarin 120 Dye. Proteins DbjA-H280F and DhaA-H272F were diluted to the final concentration 50 μ M in 50 mM phosphate buffer (pH 7.5) to a final volume of 1 mL. HaloTag Coumarin Ligand (Promega Corporation, Madison, U.S.A.) was added to the enzyme solution to a final concentration 15 μ M. Reaction was gently mixed and incubated for 15 min at 37 °C. Free coumarin is highly undesirable for the fluorescence experiments; therefore, the following steps of labeling protocol were optimized to achieve efficient removal of unbound coumarin. Three procedures for the removal of unbound dye were tested: (i) dialysis, (ii) the usage of HiTrap desalting column (Amersham Biosciences, Freiburg, Germany), and (iii) binding of the complex to HiTrap column followed by washing of the column with buffer. The final procedure was as follows (Supporting Information, Figure S1): the protein–ligand complex was loaded by syringe on 1 mL Ni-NTA HiTrap column pre-equilibrated with buffer composed of 16.4 mM K_2HPO_4 , 3.6 mM KH_2PO_4 , and 0.5 M NaCl containing 10 mM imidazole (pH 7.5). Unbound ligand was washed out with 100 mL of the buffer used for pre-equilibrating the column. The protein–ligand complex bound by six histidine tags on the C-terminus of the protein was eluted from the column with buffer containing 300 mM imidazole. The protein–ligand sample was dialysed against 20 mM glycine

buffer (pH 8.2) to remove imidazole and NaCl and was immediately used for fluorescence measurements.

Verification of Alkyl-Enzyme Intermediates in DbjA-H280F and DhaA-H272F by MALDI-TOF MS. Phosphate buffer used for purification of mutant haloalkane dehalogenases was exchanged with glycine buffer (20 mM) using HiTrap Desalting Column (Amersham Biosciences, Freiburg, Germany). The protein–ligand reaction proceeded in a volume of 10 μ L. Concentration of the ligand was adjusted to achieve 100% saturation of the enzyme. Then 1 μ L of the reaction mixture was used for MALDI-TOF MS analysis. Mass spectra of the proteins were recorded on a Reflex IV (Bruker, Bremen, Germany) operated in the linear mode with detection of positive ions. Mixture of 2,5-dihydroxybenzoic acid and 5-methoxysalicylic acid (9:1) was used as the matrix. The solution of the matrix (20 mg/mL) was prepared in 20% acetonitrile with 1% trifluoroacetic acid. The samples were mixed with the matrix solution in ratio of 1:3. The doubly charged peak of BSA was used for external mass calibration. Mass spectra were processed with XMASS 5.1.5 software (Bruker, Bremen, Germany).

Steady-State and Time-Resolved Fluorescence Measurements. Steady-state excitation and emission spectra were recorded on a Fluorolog-3 spectrofluorometer (model FL3-11; HORIBA Jobin Yvon Inc., Edison, NJ, U.S.A.) equipped with a Xenon-arc lamp at 10 °C. All spectra were collected in 1 nm steps (2 nm bandwidths were chosen for both the excitation and emission monochromators). The temperature in the cuvette holder was

maintained within ± 0.1 °C using a water-circulating bath. When performing the fluorescence quenching measurements, the samples were excited at 350 nm, and the emission was detected at 450 nm. The aliquots of the quencher solutions were added directly to the protein sample in the cuvette with a Hamilton syringe, and the cuvette contents were stirred continuously. The recorded values of the fluorescence intensity were corrected for dilution effects.

The steady-state anisotropy was measured with polarizers inserted into the setup at the same wavelength regions as for the quenching experiments. Four intensities of polarized fluorescence (I_{VV} , I_{VH} , I_{HV} , I_{HH}) were recorded, where V and H in the subscripts respectively represent the vertical and horizontal directions, and the first and second subscript denotes the direction plane of the polarization in the excitation and emission arm, respectively. The steady-state anisotropy was calculated as follows:

$$r_{st} = \frac{I_{VV} - GI_{VH}}{I_{VV} + 2GI_{VH}} \quad (1)$$

in which G is the instrumental correction factor given by the observed ratio, I_{HV}/I_{HH} .

Absorption spectra were recorded on a Perkin-Elmer Lambda 19 spectrometer (Perkin-Elmer, Wellesley, MA, U.S.A.).

Fluorescence decays were collected by using a IBH 5000 U SPC equipment (HORIBA Jobin Yvon Inc., Edison, NJ, U.S.A.) with a picosecond diode laser (IBH NanoLED 11 370 nm peak wavelength, 0.1 ns pulse width, 1 MHz repetition rate) and a cooled Hamamatsu R3809U-50 microchannel plate photomultiplier (Hamamatsu, Shizuoka, Japan) with 50-ps time resolution. Emission decays were recorded at a series of wavelengths spanning the steady-state emission spectrum (400–490 nm) in 5 nm steps. In order to eliminate scattered light, a 399 nm cutoff filter was used. The signal was kept below 2% of the light source repetition rate, and data were collected in 4096 channels (0.028 ns per channel) until the peak value reached 5000 counts. Fluorescence decays were fitted to multiexponential functions, using the iterative deconvolution procedure with IBH DAS6 software.

In order to perform the time-resolved polarization experiments, the polarizers were inserted into the IBH 5000 U spectrometer. Following the notation defined above for the steady-state anisotropy the time-resolved anisotropy decays were obtained according to:

$$r(t) = \frac{I_{vv}(t) - GI_{vh}(t)}{I_{vv}(t) + 2GI_{vh}(t)} \quad (2)$$

where G is the correction factor and t is time. The recorded decays were fitted with the formula:

$$r(t) = (r(0) - r(\infty))[a_1 \exp(-t/\phi_1) + a_2 \exp(-t/\phi_2)] + r(\infty) \quad (3)$$

here $r(0)$ and $r(\infty)$ stand for the limiting and residual anisotropy, respectively, and ϕ_i are the rotational correlation times and a_i the corresponding amplitudes.

Time-resolved emission spectra (TRES) were obtained by the spectral reconstruction method as described elsewhere.^{29–33} In order to determine the position of the spectra $\nu(t)$ (i.e., their maxima) and their full widths at half-maximum (fwhm), the TRES were fitted

by a log-normal function. The time evolution of the TRES maximum $\nu(t)$ was fitted according to:

$$\nu(t) = \nu(\infty) + (\nu(0) - \nu(\infty)) \sum_{i=1}^3 \exp(-t/\tau_i) \quad (4)$$

Correlation function $C(t)$ was calculated from the emission maxima $\nu(t)$ of the TRES at time t after excitation according to:

$$C(t) = \frac{\nu(t) - \nu(\infty)}{\nu(0) - \nu(\infty)} \quad (5)$$

where $\nu(0)$ and $\nu(\infty)$ are the emission maxima at time zero (discussed in detail in the Results) and infinity, respectively. The $\nu(\infty)$ value can be estimated by analyzing the reconstructed TRES. To characterize the overall time scale of solvent response, an average relaxation time was calculated as follows:

$$\tau_r \equiv \int_0^{\infty} C(t) dt \quad (6)$$

Preparation of Structures for Molecular Modeling. The crystal structures of the haloalkane dehalogenases DbjA³⁴ and DhaA³⁵ were obtained from RSCB PDB using the accession codes 3BSP and 1CQW, respectively. The catalytic histidines of DbjA (H280) and DhaA (H272) were substituted by a phenylalanine. Additional mutations V172A, I209L, and G292A were modeled to the crystal structure of DhaA-H272F to make it identical with the haloalkane dehalogenase DhaA used in our experiments. All mutations were designed in PyMOL 0.99.³⁶ Hydrogen atoms were added by WHAT IF 6.0.³⁷ The fluorescent probe consisting of coumarin dye carrying a covalent alkyl-halogen linker was built in PyMOL 0.99.³⁶ The geometry of the probe molecule was optimized using AM1³⁸ implemented in the program MOPAC2002. Structures of enzymes and fluorescent probes were prepared for docking calculation by MGLTools 1.5.0.³⁹ The fluorescent probe was docked into the active sites of both studied enzymes using the program AUTODOCK 3.05.⁴⁰ The atomic and electrostatic maps were calculated using AUTOGRID 3.06.⁴⁰ The range of grid maps was set to $95 \times 95 \times 95$ grid points with spacing 0.25 Å centered above substituted phenylalanine to cover the whole active sites and the main tunnels of both enzymes; 250 docking calculations were performed employing the Lamarckian Genetic Algorithm with the following parameters: initial population size 150, maximum of 1.5×10^6 energy evaluations and 27,000 generations, elitism value 1, mutation rate 0.02, and cross-over rate 0.8. The local search was based on pseudo-Solis and Wets algorithm with a maximum of 300 iterations per local search.⁴¹ Final orientations from every docking were clustered with a clustering tolerance for the root-mean-square positional deviation of 2 Å.

Quantum Mechanics/Molecular Mechanics Stochastic Boundary Molecular Dynamics (QM/MM SBMD) Simulations. The covalently bound alkyl-enzyme intermediates were modeled from the substrate–enzyme complexes obtained from the docking calculations (Figure 1). The structure was selected on the basis of knowledge of the reactive conformation in the haloalkane dehalogenases. The enzyme–substrate complex closest geometrically to

- (29) Hof, M. In *Applied Fluorescence in Chemistry, Biology, and Medicine*; Rettig, W., Strehmel, B., Schrader, S., Eds.; Springer Verlag: Berlin, 1999, pp 439–456.
- (30) Horng, M. L.; Gardecki, J. A.; Papazyan, A.; Maroncelli, M. *J. Phys. Chem.* **1995**, *99*, 17311–17337.
- (31) Hutterer, R.; Schneider, F. W.; Hermens, W. T.; Wagenvoord, R.; Hof, M. *Biochim. Biophys. Acta* **1998**, *1414*, 155–164.
- (32) Jurkiewicz, P.; Sykora, J.; Olzysnska, A.; Humplickova, J.; Hof, M. *J. Fluorescence* **2005**, *15*, 883–894.
- (33) Sykora, J.; Kapusta, P.; Fidler, V.; Hof, M. *Langmuir* **2002**, *18*, 571–574.

- (34) Sato, Y.; Natsume, R.; Tsuda, M.; Damborsky, J.; Nagata, Y.; Senda, T. *Acta Crystallogr., Sect. A* **2007**, *63*, 294–296.
- (35) Newman, J.; Peat, T. S.; Richard, R.; Kan, L.; Swanson, P. E.; Affholter, J. A.; Holmes, I. H.; Schindler, J. F.; Unkefer, C. J.; Terwilliger, T. C. *Biochemistry* **1999**, *38*, 16105–16114.
- (36) DeLano, W. L.; v0.99 ed.; DeLano Scientific LCC: San Francisco, 2006.
- (37) Vriend, G. *J. Mol. Graphics* **1990**, *8*, 52–56.
- (38) Stewart, J. J. P. *J. Comput.-Aided Mol. Des.* **1990**, *4*, 1–45.
- (39) Sanner, M. F. *J. Mol. Graphics Modell.* **1999**, *17*, 57–61.
- (40) Morris, G. M.; Goodsell, D. S.; Halliday, R. S.; Huey, R.; Hart, W. E.; Belew, R. K.; Olson, A. J. *J. Comput. Chem.* **1998**, *19*, 1639–1662.
- (41) Solis, F. J.; Wets, R. J. B. *Math. Oper. Res.* **1981**, *6*, 19–30.

the near attack configuration of S_N2 reaction in a haloalkane dehalogenase⁴² was selected, and the alkyl-enzyme intermediate was prepared by deleting the chloride atom and placing the carbon atom 1 Å closer to the oxygen atom of aspartic acid. The alkyl-enzyme intermediate was solvated by immersion into a 30 Å sphere of TIP3P water molecules.⁴³ All water molecules beyond 25 Å from the origin and those overlapping within 2.5 Å with protein and molecules of crystal water were deleted. The system was simulated with QM/MM SBMD using CHARMM c34b1.⁴⁴ The alkyl-enzyme intermediate was selected as QM region to achieve proper treatment of this region without a need for parametrization of the intermediate for which experimental data are not available. The C_β -atom of former catalytic aspartic acid was used as interface between QM and MM region according to the generalized hybrid orbital method.⁴⁵ QM region was handled by the semiempirical method AM1, while the rest of enzyme and all water molecules were described by the CHARMM22 force field.^{46,47} The system was separated into reaction, buffer, and reservoir region according to QM/MM SBMD methodology.⁴⁸ Division was as follows: atoms were selected as the reaction region if any atom within the residue was within 20 Å from the origin, residues with all atoms beyond 25 Å from the origin were selected as the reservoir region, and the remaining atoms were selected as the buffer region. Atoms in the reaction region were propagated by Newton's equations of motion, while atoms in the buffer region were treated by Langevin dynamics. Protein atoms in the buffer region were constrained by harmonic forces derived from crystallographic temperature factors.⁴⁹ The system was energetically minimized by optimizing separately water molecules, alkyl-enzyme intermediate, and alkyl-enzyme intermediate together with water molecules, while keeping the rest of the system fixed. Minimization was performed using 1000 steps of adopted basis Newton–Raphson algorithm and was followed with 5 ps dynamics of water molecules. Subsequently, the system was heated in three sequential heating MD simulations consisting of 12, 13, and 15 ps with initial and final temperature 98–150 K, 150–230 K, and 230–298 K, respectively. The overall length of the following production runs were 2 ns. During all MD simulations the settings used were as follows: the SHAKE algorithm⁵⁰ keeping all hydrogen bonds in the MM region constrained near their equilibrium distances and time step of 1 fs. A friction coefficient of 200 ps⁻¹ was used for the protein atoms, and 62 ps⁻¹ was used for the water molecules in the buffer region.

Results

Preparation of Specifically Labeled Proteins. The wild-type haloalkane dehalogenases DbjA and DhaA were mutated in the catalytic histidine by site-directed mutagenesis and overexpressed in *E. coli* BL21. Both mutant proteins DbjA-H280F and DhaA-H272F were purified into homogeneity by metal-affinity chromatography which was verified by SDS–PAGE (Supporting Information, Figure S2). The proteins DbjA-H280F and DhaA-H272F were labeled by a coumarin dye, and unbound

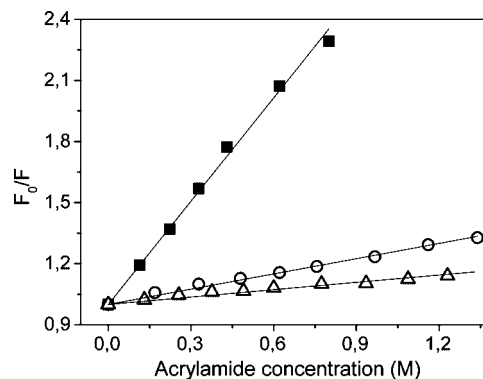


Figure 2. Stern–Volmer plots for coumarin when freely dissolved in buffer (■), coumarin-labeled DbjA-H280F (○), and coumarin-labeled DhaA-H272F (△). The obtained Stern–Volmer constants K_{sv} are 1.64, 0.25, and 0.12 M⁻¹, respectively. Solid lines represent the linear fits.

fluorescent dye was removed by an optimized protocol, which is critical for the quality of solvent relaxation experiments: (i) the complex was bound on a metal-affinity column, and unbound dye was removed by a washing buffer using the equivalent of 100 dead volumes of a column, and (ii) the salts originating from washing buffer were removed from a sample by dialysis (Supporting Information, Figure S1). Dialysis alone or the use of desalting column led to a faster quenching rate and significantly faster solvent relaxation behavior, indicating the presence of the free or nonspecifically bound coumarin in the sample. The same effect was observed when a too-low amount of washing buffer was applied to remove the free coumarin from the complex bound on a HiTrap column (Supporting Information, Figures S3,4). Formation of the alkyl-enzyme intermediates in DbjA-H280F and DhaA-H272F prepared by the optimized protocol was verified by MALDI-TOF MS analysis. The difference of average masses of modified and unmodified proteins corresponds to the mass of bound coumarin dye. Comparison of molecular weights of mutant haloalkane dehalogenase and the same protein with the fluorescent probe confirmed that DbjA-H280F and DhaA-H272F incorporated coumarin in their structures. The results of MALDI-TOF MS analysis of DbjA-H280F with coumarin dye are shown in the Supporting Information, Figure S5.

Acrylamide Quenching. To verify that the majority of the fluorescence signal originates from coumarin dye attached to the protein, the acrylamide quenching experiments were performed for coumarin dye freely dissolved in the buffer, and mutants DbjA-H280F and DhaA-H272F labeled with coumarin. As is obvious from Figure 2, the Stern–Volmer plots for all the investigated systems are linear. Figure 2 illustrates vast differences among the free coumarin in the buffer and the enzyme-label assays. In comparison to the coumarin freely present in the solution, the obtained Stern–Volmer constants are 4- and 10-fold lower for DbjA-H280F and DhaA-H272F, respectively. These values prove that the coumarin dye is indeed shielded from the reach of the quencher by the protein backbone. Moreover, the emission spectra are not altered even at the high concentrations of the acrylamide for either of the enzyme mutants (Supporting Information, Figure S3), indicating that more fractions of the dye with a different accessibility to the quencher are not present, nor are there completely different microenvironments present at the same moment. In addition, the coumarin attached to DhaA-H272F shows slightly lower accessibility to the quencher molecules than DbjA-H280F.

(42) Hur, S.; Kahn, K.; Bruice, T. C. *Proc. Natl. Acad. Sci. U.S.A.* **2003**, *100*, 2215–2219.

(43) Jorgensen, W. L.; Chandrasekhar, J.; Madura, J. D.; Impey, R. W.; Klein, M. L. *J. Chem. Phys.* **1983**, *79*, 926–935.

(44) Brooks, B. R.; Brucoleri, R. E.; Olafson, B. D.; States, D. J.; Swaminathan, S.; Karplus, M. *J. Comput. Chem.* **1983**, *14*, 187–217.

(45) Gao, J. L.; Amara, P.; Alhambra, C.; Field, M. J. *J. Phys. Chem.* **1998**, *102*, 4714–4721.

(46) MacKerell, A. D.; et al. *J. Phys. Chem.* **1998**, *102*, 3586–3616.

(47) MacKerell, A. D., Jr.; Feig, M.; Brooks, C. L., III. *J. Comput. Chem.* **2004**, *25*, 1400–1415.

(48) Brooks, C. L., III.; Brunger, A.; Karplus, M. *Biopolymers* **1985**, *24*, 843–865.

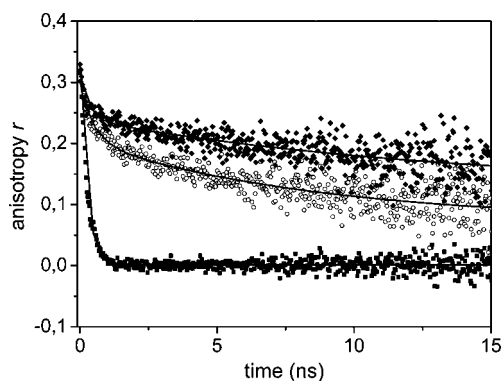
(49) Brunger, A. T.; Brooks, C. L., 3rd.; Karplus, M. *Proc. Natl. Acad. Sci. U.S.A.* **1985**, *82*, 8458–8462.

(50) Ryckaert, J. P.; Ciccotti, G.; Berendsen, H. C. *J. Comput. Phys.* **1977**, *23*, 327–341.

Table 1. Parameters Gained from the Steady-State Anisotropy Measurements and from the Fitting of the Time-Resolved Anisotropy Decays^a

	r_{st}	r_0	r_∞	ϕ_1 (ns) (a_1)	ϕ_2 (ns) (a_2)
coumarin	0.02	0.28	0.00	0.1	—
DbjA-H280F	0.19	0.28	0.09	0.3 (0.05)	7.4 (0.95)
DhaA-H272F	0.25	0.29	0.14	0.2 (0.02)	10.3 (0.98)

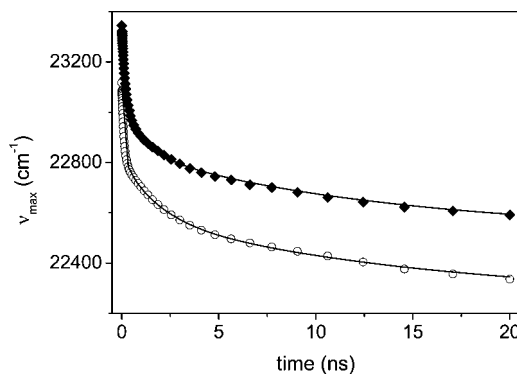
^a r_{st} stands for the steady-state anisotropy, r_0 for the limiting anisotropy, r_∞ for the residual anisotropy, ϕ_i for the rotational correlation times, and a_i amplitudes (weighted by the rotational correlation times).

**Figure 3.** Time-resolved anisotropy decays of coumarin freely dissolved in water (■), and two labeled mutants DbjA-H280F (○) and DhaA-H272F (◆). Solid lines represent the fits according to formula 3.

Anisotropy. The values obtained by the steady-state and time-resolved anisotropy are summarized in Table 1. Similarly to the quenching experiments there is a significant difference between the coumarin freely dissolved in water and the dehalogenase mutants labeled with coumarin. The latter system has significantly higher values for the steady-state anisotropy and slower correlation times, proving that the coumarin label is attached to the protein. There is also a slight difference between the DbjA-H280F and DhaA-H272F. The coumarin embedded in DhaA-H272F shows higher values of the steady-state anisotropy (Table 1) and slower rotational diffusion (Figure 3).

Time-Resolved Emission Spectra (TRES). The crucial step for the proper determination of the overall time-dependent Stokes shift (TDSS), which is directly related to the micropolarity of the dye microenvironment, and the relaxation residence times, which reflect the microviscosity of the dye microenvironment, is the so-called “Time 0 estimation”, i.e. the determination of the spectrum which is emitted prior to the occurrence of any solvent relaxation. As published by Pal et al.,⁵¹ coumarin 120 exhibits unusual complex photophysics in the nonpolar solvents. Therefore, the standard procedure suggested by Maroncelli⁵² fails. The alternative approach has to be used as depicted in Supporting Information, Figure S6.

Having known the “Time 0 spectrum”, the time-resolved emission spectra were recorded for both DbjA-H280F and DhaA-H272F mutants labeled with coumarin. As is obvious from Figure 4 and Table 2, the overall Stokes shift is significantly smaller for the DhaA-H272F mutant, indicating a lower mi-

**Figure 4.** Time evolution of TRES peak maxima $\nu(t)$ for coumarin-labeled DbjA-H280F (○) and DhaA-H272F (◆) mutants. Solid lines represent the multiexponential fits according to formula 4.**Table 2.** Parameters Gained by the Multiexponential Fitting of Time Evolution of the TRES Peak Maximum $\nu(t)$, “Time 0 Estimation”, and Analysis of the Autocorrelation Curve $C(t)$ ^a

	$\nu(\infty)$ (cm^{-1})	$\Delta\nu_{\text{eff}}$ (cm^{-1})	τ_1 (ns) (A_1)	τ_2 (ns) (A_2)	τ_3 (ns) (A_3)	ν_0 (cm^{-1})	$\Delta\nu$ (cm^{-1})	τ_r (ns)	% obs
DbjA-H280F	22100	900	<0.1 (280)	1.4 (220)	11 (370)	23400	1300	2.8	70
DhaA-H272F	22350	850	0.2 (310)	1.3 (340)	12.6 (200)	23300	950	4.1	90

^a $\nu(\infty)$ stands for the fitted value for $t \rightarrow \infty$, $\Delta\nu_{\text{eff}}$ is the difference between the very first point gained by the spectral reconstruction and $\nu(\infty)$, τ_i are the fitted relaxation times, A_i correspond to the amplitudes, ν_0 stands for “time 0 estimation”, $\Delta\nu$ is the overall Stokes shift ($\Delta\nu = \nu_0 - \nu(\infty)$), τ_r is the integral relaxation time, and % obs corresponds to the percentage of the solvent relaxation process captured with the given experimental time resolution of 50 ps (% obs = $100\Delta\nu_{\text{eff}}/\Delta\nu$).

cropolarity of the dye microenvironment. It might be caused by a lower amount of the water molecules or the presence of some more hydrophobic amino acid residues in the vicinity of the coumarin label attached to DhaA-H272F. The multiexponential fitting of the time evolution of TRES maxima $\nu(t)$ provides the residence times for both mutants on the similar time scales, i.e. on the order of 100 ps, of 1 ns, and on the order of 10 ns. Such a complex behavior spread over the large time window has already been reported on the solvation dynamics in the protein interior several times.^{15,17,53} By comparing the value of the “time 0 estimation” and the very first value obtained by the spectral reconstruction we can quantify what part of the solvent relaxation is captured. Herein we observe 70% and 90% of the overall relaxation process with the experimental resolution of 50 ps for DbjA-H280F and DhaA-H272F, respectively. The kinetics of the TDSS response is even so slow, that the relaxation process is not complete within the experimental time window (~ 20 ns), which is given by the fluorescence lifetime of the coumarin dye. Unfortunately, this fact does not allow for the proper construction of the correlation function $C(t)$. Nevertheless, in order to get a rough idea of the kinetics of the solvent relaxation process we used the value of $\nu(t \rightarrow \infty)$, which is a limit for time infinity of the exponential fit to the time dependence $\nu(t)$. The integral relaxation time is increased from 2.8 ns for DbjA-H280F up to 4.1 ns for DhaA-H272F, which indicates that the microenvironment of the coumarin attached to DhaA-H272F is less mobile than in the case of DbjA-H280F. Nevertheless, the obtained values cannot be taken absolutely and are meant only for the comparison.

(51) Pal, H.; Nad, S.; Kumbhakar, M. *J. Chem. Phys.* **2003**, *119*, 443–452.

(52) Fee, R. S.; Maroncelli, M. *Chem. Phys.* **1994**, *183*, 235–247.

(53) Jordanides, X. J.; Lang, M. J.; Song, X. Y.; Fleming, G. R. *J. Phys. Chem. B* **1999**, *103*, 7995–8005.

We can conclude from the fluorescence experiments that the coumarin is attached to the protein specifically and there are no indications that another dye location contributes to the recorded data. In addition, there exist distinct differences in the properties of the coumarin microenvironment at the interior of the two dehalogenase mutants, DbjA-H280F and DhaA-H272F. In the case of DhaA-H272F, the coumarin is less accessible to the quencher and has a lower motional freedom, and its microenvironment exhibits lower micropolarity and higher microviscosity compared to DbjA-H280F.

Molecular Modeling. QM/MM SBMD simulations were stable based on steady values of root-mean-square deviation, radius of gyration of enzyme, and total, potential, and kinetic energy of the system (data not shown). Low deviations, low fluctuation, and rapid equilibration can be related to constraints applied to our system simulated by QM/MM SBMD methodology. Formation of van der Waals contacts between the fluorescent dye and two amino acid residues for more than 75% of simulation time was observed in both systems. The total number of residues showing van der Waals contacts with the dye for the shorter part of the simulation time is, however, different (Supporting Information, Table S1). The composition of the residues in close proximity to the dye in DbjA-H280F is more variable than that in DhaA-H272F, which correlates with the higher mobility of the coumarin dye and higher values of *B*-factors (Figure 5). The higher motional freedom of the region located near the bound dye and the dye itself forces the hydration layer around the probe to behave with less viscosity in DbjA-H280F than in DhaA-H272F (Table 3). The enzyme flexibility is partially influenced by the interactions with the bound probe. Analysis of the *B*-factors of free and complexed enzymes reveals that binding of the probe makes DhaA-H272F enzyme more rigid with the significant exception of four residues (Ala151, Phe152, Arg153, and Thr154) located in the loop between α 4 and α 5. This loop was found to be more flexible in the complexed enzyme. The residues closest to the dye in DbjA-H280F enzyme were generally more flexible than in the free enzyme (Figure 5). The most significant increase in flexibility was observed in the helix α 4 and in the loop carrying the mutation His280Phe. This difference could be due to higher motional freedom of the bound probe and its linker located in the wider main tunnel of DbjA-H280F (Figure 1). On the contrary, interactions with the fixed probe in DhaA-H272F contribute to the overall stabilization of the entire complex. The main tunnel is more narrow in the DhaA-H272F enzyme than in DbjA-H280F, which makes the linker of the dye straighter and the dye itself more exposed to the surrounding solvent (Table 3, Figure 1). In both enzymes, the fluorescent probe binds in such a way that the coumarin moiety is exposed to the solvent while the linker fills up the main tunnel and prevents exchange of water molecules between the active site and bulk solvent. The amino acid residues located in the vicinity of the coumarin moiety in DhaA-H272F are generally more hydrophobic and, together with lower hydration of the dye, results in lower polarity of the microenvironment (Table 3). This finding is further supported by lower total dipole moment of the microenvironment of the fluorescent probe bound to DhaA-H272F (Table 3).

Concluding Discussion

We propose a novel protocol for labeling of the dehalogenase enzyme with the fluorescent coumarin dye which serves as a substrate for the enzymatic reaction. In this way the tunnel

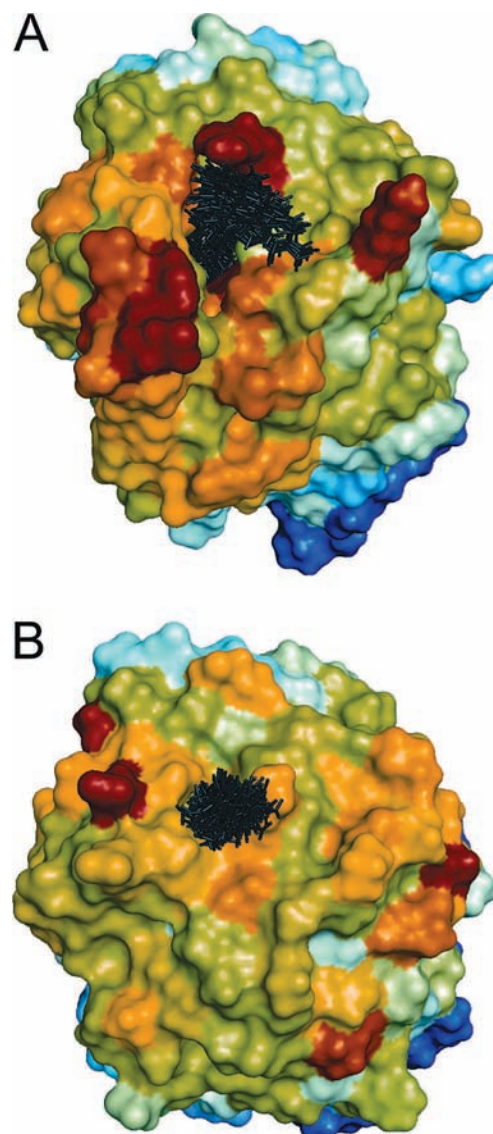


Figure 5. Population of the coumarin probe (black sticks) observed in DbjA-H280F (A) and DhaA-H272F (B) during MD simulations. The color scale indicates flexibility of the residues quantified by *B*-factors as follows: dark blue < light blue < green < yellow < orange < red.

mouths of DbjA-H280F and DhaA-H272F are labeled specifically as the unbound and nonspecifically bound coumarin is removed from the sample. Acrylamide-quenching experiments confirm the selective labeling, and docking experiments reveal the location of the coumarin dye at the tunnel mouths. Quenching experiments and time-resolved anisotropy measurements show that the coumarin label is probing environments with different properties in each enzyme. For DhaA-H272F we determine smaller accessibility of the dye to the quencher molecules and lower motional freedom of the chromophore than for DbjA-H280F. These findings are in line with a narrower tunnel in DhaA-H272F, compared to that of DbjA-H280F. TDSS experiments again show significant differences. DhaA-H272F shows lower hydration and slower mobility of amino acid residues surrounding the probe. This observation is in accordance with solvent dipole moments and diffusion coefficients obtained by QM/MM SBMD simulations. Moreover, the course of TDSS was found to be remarkably slow, occurring almost exclusively on the nanosecond time scale even though the dye is located directly at the tunnel mouth of the enzyme,

Table 3. Comparison of Parameters Characterizing the Coumarin Dye and its Microenvironment in DbjA-H280F and DhaA-H272F Obtained by the QM/MM SBMD Simulations and by the Fluorescence Experiment (*in italics*).

parameter	enzyme		interpretation
	DbjA-H280F	DhaA-H272F	
density of solvent (5 Å around dye) [kg·m ⁻³]	3.65	1.16	higher hydration of dye in DbjA-H280F
<i>dynamic Stokes shift</i> [cm ⁻¹]	<i>1300</i>	<i>950</i>	
average total dipole momentum of solvent and protein within 5 Å around dye [D]	55.94	42.98	microenvironment of the dye is more polar in DbjA-H280F
<i>dynamic Stokes shift</i> [cm ⁻¹]	<i>1300</i>	<i>950</i>	
root mean square fluctuation of the dye [Å ²]	2.22	2.15	the dye is more flexible in DbjA-H280F
<i>mean rotational correlation time</i> ϕ_{av}^a [ns]	<i>7.4</i>	<i>10.3</i>	
diffusion coefficient of solvent within 5 Å around dye [Å ² ·ps ⁻¹]	0.0084	0.0047	solvent around the dye is more viscous in DhaA-H272F
<i>integral relaxation time</i> τ_r [ns]	<i>2.8</i>	<i>4.1</i>	

^a ϕ_{av} was calculated from the parameters presented in Table 1 according to the equation: $\phi_{av} = (a_1\phi_1^2 + a_2\phi_2^2)/(a_1\phi_1 + a_2\phi_2)$.

i.e. in the vicinity of the protein surface. This finding indicates that the protein dynamics at the tunnel mouth, which is probed by the nanosecond TDSS, is significantly slowed down compared to the nonbiologically relevant regions of the protein⁵ to maintain the proper functioning of the enzyme. In our case, we believe that the nanosecond dynamics helps to control the proper access of the substrates and release of the products from buried active sites of the haloalkane dehalogenase.

In summary we find clear differences in structure, hydration, and dynamics of these mouth openings. Recent evolutionary analysis of the protein family of haloalkane dehalogenases revealed that this region is the most variable among haloalkane dehalogenases originating from different bacterial species,⁵⁴ suggesting its importance for adaptation of enzymes to various substrates. Moreover, it has been shown that the exchange of ligands between bulk solvent and occluded active site can limit the overall reaction rate of haloalkane dehalogenases^{55,56} and that the reaction rate as well as substrate specificity can be modulated by the mutations introduced to the tunnel mouth.⁵⁷ Thus, we have good reasons to believe that the presented

findings are relevant for structure–function relationships of these proteins. Additional studies, currently ongoing in our laboratories, are needed for better understanding of the importance of tunnel mouth dynamics for functional properties of enzymes with buried active sites.

Acknowledgment. Financial support of the Grant Agency of the Czech Republic via 203/08/0114 (M.H., J.D.), the Ministry of Education, Youth and Sports of the Czech Republic via LC06063 (J.S.), LC06010 (J.B.), MSM0021622412 (J.D.), MSM0021622413 (A.J.) and MSM0021622415 (Z.Z.) is gratefully acknowledged. The access to the METACentrum supercomputing facilities provided under the research intent MSM6383917201 is acknowledged.

Supporting Information Available: Scheme of optimized protocol for specific labeling of haloalkane dehalogenases; SDS–PAGE of purified haloalkane dehalogenases mutated in catalytic histidine; emission spectra of labeled dehalogenase before and after the acrylamide quenching; Stern–Volmer plots for labeled dehalogenase; MALDI–TOF MS spectra of free and complexed haloalkane dehalogenases; dependence of the Stokes shift $\Delta\nu_{AE}$ on the polarity function for coumarin 120; description of the “time 0 estimation” procedure; list of residues making van der Waals contacts with the coumarin dye; complete ref 46. This material is available free of charge via the Internet at <http://pubs.acs.org>.

JA804020Q

- (54) Chovancova, E.; Kosinski, J.; Bujnicki, J. M.; Damborsky, J. *Proteins: Struct., Funct., Bioinf.* **2007**, *67*, 305–316.
 (55) Bosma, T.; Pikkemaat, M. G.; Kingma, J.; Dijk, J.; Janssen, D. B. *Biochemistry* **2003**, *42*, 8047–8053.
 (56) Schanstra, J. P.; Janssen, D. B. *Biochemistry* **1996**, *35*, 5624–5632.
 (57) Chaloupkova, R.; Sykorova, J.; Prokop, Z.; Jesenska, A.; Monincova, M.; Pavlova, M.; Tsuda, M.; Nagata, Y.; Damborsky, J. *J. Biol. Chem.* **2003**, *278*, 52622–52628.